Energy, metastability, and optical properties of anion-disordered R Ox H3-2x (R= Y, La) oxyhydrides

A computational study

Colombi, Giorgio; Stigter, Rens; Chaykina, Diana; Banerjee, Shrestha; Kentgens, Arno P.M.; Eijt, Stephan W.H.; Dam, Bernard; De Wijs, Gilles A.

DOI
10.1103/PhysRevB.105.054208

Publication date
2022

Document Version
Final published version

Published in
Physical Review B

Citation (APA)
Colombi, G., Stigter, R., Chaykina, D., Banerjee, S., Kentgens, A. P. M., Eijt, S. W. H., Dam, B., & De Wijs, G. A. (2022). Energy, metastability, and optical properties of anion-disordered R Ox H3-2x (R= Y, La) oxyhydrides: A computational study. *Physical Review B*, *105*(5), Article 054208. https://doi.org/10.1103/PhysRevB.105.054208

Energy, metastability, and optical properties of anion-disordered RO_xH_{3-2x} (R = Y, La) oxyhydrides: A computational study

Giorgio Colombi,[1,*] Rens Stigter,[2,3] Diana Chaykina,[1,2] Shrestha Banerjee,[4] Arno P. M. Kentgens,[4] Stephan W. H. Eijt,[2] Bernard Dam,[1] and Gilles A. de Wijs[4]

[1]*Materials for Energy Conversion and Storage, Department of Chemical Engineering, Delft University of Technology, Van der Maasweg 9, NL-2629HZ Delft, The Netherlands*

[2]*Fundamental Aspects of Materials and Energy, Department of Radiation Science and Technology, Faculty of Applied Sciences, Delft University of Technology, Mekelweg 15, NL-2629 JB Delft, The Netherlands*

[3]*Process and Energy Department, Delft University of Technology, Mekelweg 2, NL-2628CD Delft, The Netherlands*

[4]*Radboud University, Institute for Molecules and Materials, Heyendaalseweg 135, NL-6525 AJ Nijmegen, The Netherlands*

(Received 14 November 2021; accepted 27 January 2022; published 22 February 2022)

In this paper, we investigate by *ab initio* DFT how the O:H ratio influences the formation and lattice energy, metastability, and optical properties of Y and La anion-disordered RO_xH_{3-2x} oxyhydrides. To achieve this, a set of special quasirandom structures (SQS) is introduced to model anion-disorder along the whole $RH_3 - R_2O_3$ composition line. A comparison with an extensive set of anion-ordered polymorphs of the same composition shows the comparable energy of the anion-disordered phase, which, in particular, in the H-rich composition interval showed the lowest relative energy. In turn, the metastability of the anion-disordered phase depends on the cation size (Y versus La), which determines the maximum H content above which the CaF_2-type structure itself becomes unstable. To overcome the accuracy limitations of classical DFT, the modified Becke-Johnson (mBJ) scheme is employed in the study of the electronic properties. We show that major differences occur between H-rich and O-rich R oxyhydrides, as the octahedral H^- present for $x < 1$ form electronic states at the top of the valence band, which reduce the energy band gap and dominate the electronic transitions at lower energies, thus increasing the refractive index of the material in the VIS-nIR spectral range. Comparing the DFT results to experimental data on photochromic Y oxyhydride films reinforces the hypothesis of anion-disorder in the H-rich films ($x < 1$), while it hints towards some degree of anion ordering in the O-rich ones ($x > 1$). Our paper exemplifies a strategy to calculate *ab initio* the electronic/optical properties of a wide range of materials with occupational disorder.

DOI: 10.1103/PhysRevB.105.054208

Rare-earth (R) oxyhydrides, RO_xH_{3-2x}, are gaining attention in view of their fast hydride ion conductivity [1] and peculiar optoelectronic behavior (i.e., large reversible photoconductivity and photochromism) [2–4], properties that hold promises for electrochemical devices, such as solid-state batteries and fuel cells [5], as well as smart coatings for windows and sensors.

R oxyhydrides are *mixed-anion* compounds, a class of inorganic materials, which offers unprecedented degrees of freedom in the design of functional properties thanks to the broad spectrum of different anion characteristics (e.g., electronegativity, polarizability, ionic radii) and the possibility to tune the anion-ratio within a wide compositional interval [6,7]. From a structural perspective, this large compositional flexibility is reflected in a variety of stable and metastable phases. In addition, given the comparable ionic radii of O^{2-} (140 pm) and H^- (120–150 pm) [6] in R oxyhydrides the anions can either order periodically (anion-order), or randomly share the same anion sites available within the R cation lattice (anion-disorder) [8,9].

While many anion-ordered polymorphs were reported for stoichiometric ROH ($x = 1$) [1,9–11], it is thought that anion-disorder is energetically favorable in the case of smaller cations [8,12] and outside this 1:1:1 composition [9].

The anion-disordered phase resembles the structure of CaF_2, with a face-centred cubic [3,12] or tetragonal [9] cation lattice and distinct tetrahedral and additional (less stable) octahedral anion sites. As visualized in Fig. 1, the occupation of the anion sites depends on the composition: For $x \geqslant 1$, there are enough tetrahedral sites to host all anions, while for $x < 1$ the tetrahedral sites are completely occupied with O^{2-} and H^- and the remaining fraction of H^- sits in the octahedral sites [13].

Notably, high hydride conductivities are observed in H-rich ($x < 1$) LaO_xH_{3-2x} with anion-disordered structure [1], an aspect clarified by the same authors in a second publication [9]. Similarly, Sc, Y, and Gd oxyhydride thin films show stronger photochromism for R:O:H ratios far from the

*Corresponding author: g.colombi@tudelft.nl

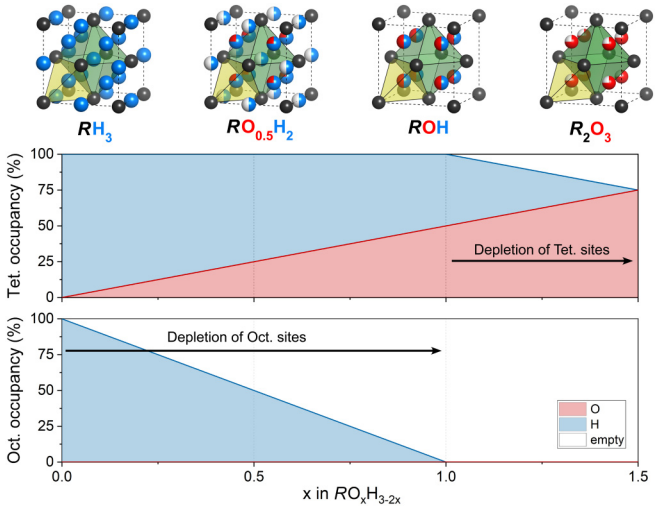

FIG. 1. Trend upon O:H ratio of the occupation of tetrahedral (yellow polygon) and octahedral (green polygon) anion sites in anion-disordered RO_xH_{3-2x} oxyhydrides with CaF_2-type structure [13]. Colour scheme: *R*, black; O, red; H, blue.

1:1:1 composition ($x = 1$) [4]. The anion-disordered phase in the H-rich range of compositions is therefore of primary importance for applications in electrochemical devices and optics.

From the point of view of anion dynamics, the link between functional properties and the underlying composition/structure has been subject of speculation. It is thought that the energy landscape for H^- site hopping influences the kinetics of hydride conduction [12], as well as the speed of the photochromic effect [4]. Direct information concerning trajectories and rates of H^- hopping are however difficult to obtain; insight is scattered, and only based on 1:1:1 *R*OH. For this composition, Ubukata *et al.* [12] proposed that H^- migrates preferentially via the so-called indirect route (i.e., from tetrahedral to octahedral site) passing through a triangular bottleneck whose size defines the activation energy of the hop. This barrier is typically found on the order of 1–1.3 eV for $P4/nmm$ LaOH and NdOH anion-ordered oxyhydrides [1,12,14]. Conversely, anion-disorder was shown to suppress H^- mobility in *R*OH [12]. The apparent contradiction with the high H^- conductivity of anion-disordered H-rich La oxyhydrides indicates that the properties of the 1:1:1 *R*OH case do not necessarily reflect those of RO_xH_{3-2x} with varying O:H composition. For example, one might expect different migration pathways for H-rich oxyhydrides, such as the direct octahedral to octahedral route.

From a computational perspective, anion-disorder introduces an additional level of complexity. A quantitative evaluation of the energy landscape for H^- hopping in anion-disordered *R* oxyhydrides is still missing, as well as for the formation energy of the vacancies that might assist its diffusion. Additionally, it remains largely unclear how material properties, such as energy, phase-stability, band structure, and optical absorption/refraction, depend on the O:H ratio.

To address this knowledge gap, we introduce here a set of special quasirandom structures (SQS) that, while maintaining a computationally affordable size, are able to model the disordered anion sublattice along the entire $RH_3 - R_2O_3$ composition line. We assess the predictive ability of the SQS approach, and discuss how the O:H ratio defines the total energy, metastability, and optical properties of Y and La anion-disordered oxyhydrides. We chose Y and La as case studies because their (ionic) radii lie at different ends of the Lanthanoid series, and their 1:1:1 oxyhydrides have been reported as anion-disordered H^- insulators (Y) and anion-ordered H^- conductors (La), respectively [8,12].

Finally, we compare the results of this computational study to (i) the experimental phase diagrams recently proposed for Y and La oxyhydrides [9], and (ii) to the optical data available for reactively-sputtered Y oxyhydride thin films [3,15,16]. In this latter case, where there is no direct information concerning the anion sublattice of the material, our paper reinforces the hypothesis of anion-disorder in H-rich YO_xH_{3-2x} thin films ($x < 1$), while, at the same time, it hints towards some degree of anion ordering in the O-rich ones ($x > 1$).

I. COMPUTATIONAL DETAILS

A. Structural models

While our focus is specifically on the anion-disordered oxyhydrides, in this paper we compare three different sets of structures to provide a broader overview and consistently compare anion-disordered and anion-ordered structures.

The first set [Fig. 2(a)]includes anion-ordered structures experimentally reported, such as the binary RH_3 trihydrides ($P6_3/mmc$, $Fm\bar{3}m$) and R_2O_3 sesquioxides ($P\bar{3}m1$, $I\bar{3}a$), and the three space groups observed for 1:1:1 Y and La oxyhydrides ($P4nmm$ [1], $P2_1/m$ [9], $Pnma$ [10]).

The second set (Fig. 2(b), and Fig. S1 in the Supplemental Material, SM [17]), is a group of hypothetical structures that we investigate to supplement the lack of information on anion ordering outside the stoichiometric *R*OH compound and the binary extremes of the RO_xH_{3-2x} line. For $x \neq 0, 1, 1.5$ it is unclear *how* the anions might order inside the tetrahedral and octahedral interstitial sites available within the CaF_2-type cation lattice. Therefore we built all schemes of anion ordering that are possible within one fcc unit cell (4 *R* atoms, 8 tetrahedral anion sites, 4 octahedral anion site). Since we showed in our previous paper that the tetrahedral sites are energetically favoured compared to the octahedral ones, and that the O^{2-} anions occupy exclusively the tetrahedral sites even in H-rich compositions [13], these constraints were taken into account. The resulting anion-ordered structures are not yet comprehensive, as they do not survey ordering schemes extending beyond one fcc unit cell.

Finally, in the third set (Fig. 2(c), and Figs. S2 and S3 in the SM [17]) we model anion-disordered oxyhydrides as special quasirandom structures (SQS), i.e., relatively small supercells that mimic the most relevant radial correlations, and thus properties, of oxyhydrides with a perfectly random anion sublattice [18]. The mcsqs code [19], as implemented in the Alloy Theoretic Automated Toolkit [20], was used to generate SQS for several O:H anion ratios (x = 0.25, 0.50, 0.75, 0.875, 1, 1.25, 1.375, and 1.5) covering the entire RO_xH_{3-2x} composition line, from RH_3 to R_2O_3. The same constraints as

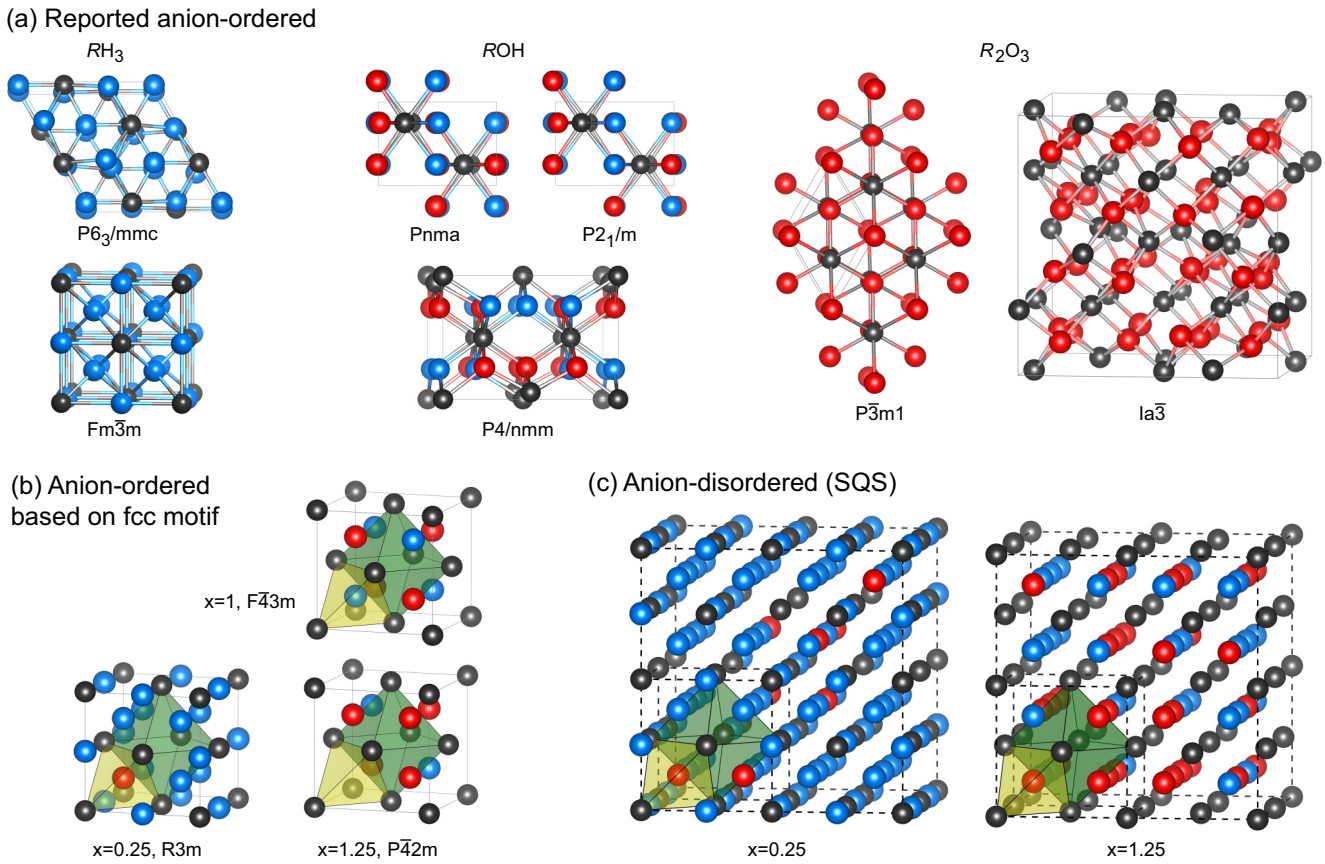

FIG. 2. Selected examples of the structures considered in this paper. Colour scheme: *R*, black; O, red; H, blue. (a) Previously reported anion-ordered compounds. This includes the binary RH_3 trihydride ($P6_3/mmc$, $Fm\bar{3}m$) and R_2O_3 sesquioxide ($P\bar{3}m1$, $I\bar{3}a$), and the 1:1:1 *R*OH oxyhydride ($P4/nmm$, $Pnma$, and $P2_1/m$). The structural difference between $Pnma$ and $P2_1m$ is minimal, and in the figure it appears as a minor translation of the anions relative to each other. (b) Examples of anion-ordered oxyhydrides based on the CaF_2 motif. Here, the anions preferentially occupy the tetrahedral sites (yellow polygons), while the octahedral ones (green polygons) only host the excess hydrogen for $x < 1$. In this paper we considered all schemes of anion ordering that are possible within one fcc unit cell. The three structures here reported are the only ones that resulted in an energy stabilization compared to the anion-disordered lattice, in view of their particular symmetry that mitigates Coulomb repulsion between neighboring O^{2-} anions. In $R3m$-$RO_{0.25}H_{2.5}$ the only octahedral empty site is adjacent to the only oxygen atom; in $F\bar{4}3m$-*R*OH the anions alternate throughout the tetrahedral sites; and in $P\bar{4}2m$-$RO_{1.25}H_{0.5}$ all the next-nearest neighbours of the empty tetrahedral site are oxygen anions. (c) Examples of special-quasirandom-structures to model anion-disordered RO_xH_{3-2x} oxyhydrides.

mentioned above were forced during the generation of SQS. Quantitatively, one estimates the goodness of an SQS via the so-called objective function (Table S1 in the SM [17]), which measures how well the radial correlations of the SQS match those of the ideal disordered structure. However, different physical properties converge at a different speed against the goodness of the SQS, and a qualitative discussion is better done in hindsight. In this paper, we considered 3 different SQS for each O:H ratio (2 in case of $x = 0.75, 1, 1.375$) so to quantify the uncertainty ($(max - min)/2$) of each of the physical quantities here reported. Hereafter, we refer to the SQS as disordered structures.

B. Structural optimization and energy

First-principle density functional theory (DFT) calculations are carried out with the Vienna *ab initio* simulation package (VASP) [21,22]. Within the scheme of the projector augmented wave (PAW) method [23,24], a plane-wave basis set is used and periodic boundary conditions are applied. Standard frozen core PAW potentials are used, and the H 1s, O 2s2p, Y 4s4p4d5s, and La 5p5d6s are treated as valence shells. For self consistent electronic calculations, as well as ionic relaxation runs, we employ the PBE generalized gradient approximation for the exchange-correlation functional [25,26]. Integrations over the Brillouin zone are performed on a Γ-centred K mesh ($8 \times 8 \times 8$ for smaller cells and $3 \times 3 \times 3$ for SQS supercells) using a Gaussian smearing of 0.05 eV. For each structure, all cell parameters and atomic positions are simultaneously optimized, reaching convergence ($\delta E <$ 0.1 meV) with a kinetic energy cut-off of 850 eV.

To avoid ill-defined values of absolute energy, only energy differences are considered in this paper. According to Hess's law, the formation energy (ΔH_f) is quantified by subtracting the energy of the isolated elements in their standard state ($P6_3/mmc$-*R*, O_2, H_2), and the binding energy (ΔH_b) is quantified by subtracting the energy of the isolated atoms. Exploiting the Born-Haber cycle, the lattice energy (ΔH_L) is

finally estimated as the sum of binding energy, experimental *R* ionization energies [27], and experimental O and H electron affinities [28] (details in the SM [17]).

The lattice energy extracted by DFT is then compared to the one predicted by the Born-Landé equation [Eq. (2), see text]. The first term of this equation, the Madelung energy, is calculated using MADEL, an application implemented in VESTA [29]. The code employs an Ewald summation [30] in the Fourier space, for which the radius of the ionic sphere was chosen to be slightly smaller than the shortest interatomic distance, and the reciprocal space range was set to 6 $Å^{-1}$. The convergence of the Madelung energy upon variation of both parameters was verified.

C. Optical properties

To overcome the limits of classical GGA-DFT, modified Becke-Johnson (mBJ) exchange potentials in combination with L(S)DA-correlation have been used to compute the electronic properties of the structures previously relaxed using PBE [31,32]. The mBJ approach has been chosen because it yields a description of the electronic states of comparable accuracy [32] to *GW* methods [33–36], while being computationally far less expensive and, thus, employable also for the larger SQS structures. A validation of mBJ results against G_0W_0 was carried for several anion-ordered Y oxyhydrides, confirming a good agreement along the whole YH_3-Y_2O_3 composition line (see Fig. S4 in the SM [17]). To extract the partial electron density-of-states (pDOS) and direct/indirect band gaps, the same kinetic energy cut-off (850 eV) and integration parameters used for PBE-DFT were maintained during the mBJ runs.

The calculation of the complex interband dielectric function, $\varepsilon(\omega) = \varepsilon_1(\omega) + i\varepsilon_2(\omega)$, is performed in the independent particle approximation, neglecting local fields and accounting only for direct transitions ($|\mathbf{q}| \to 0$). In this limit, which largely represents the dielectric properties probed at room temperature by optical spectroscopy, the imaginary part $\varepsilon_2(\omega)$ reads [37]:

$$\varepsilon_2(\omega, \hat{\mathbf{q}}) = \frac{8\pi e^2}{V} \lim_{|\mathbf{q}|\to 0} \frac{1}{|\mathbf{q}|^2} \sum_{vc\mathbf{k}} |\langle \psi_{c,\mathbf{k}+\mathbf{q}} | \psi_{v,\mathbf{k}} \rangle|^2 \times \delta(E_{c,\mathbf{k}+\mathbf{q}} - E_{v,\mathbf{k}} - \hbar\omega) \quad (1)$$

where V is the volume of the unit cell, $\hat{\mathbf{q}}$ the direction of the momentum transfer, $(v, \mathbf{k})$ and $(c, \mathbf{k}+\mathbf{q})$ indicate occupied (valence) and unoccupied (conduction) single-particle states, E their energy, and ψ the cell-periodic part of their wave functions. The real part of the dielectric function is found by Kramers-Kronig transformation of the imaginary part. To maintain analogy with the experimental data based on polycrystalline samples, in this paper we report directionally-averaged (i.e., over $\hat{\mathbf{q}}$) dielectric functions $\varepsilon(\omega)$. The convergence of $\varepsilon(\omega)$ was checked with respect to energy cut-off, K mesh, and number of computed unoccupied states. We find an optimum trade off between accuracy (i.e., invisible differences in the scale of the figures of this paper) and computational expense for a kinetic energy cut-off of 400 eV and a total of 2000 bands. K mesh and Gaussian smearing are maintained equal to the structural optimization runs.

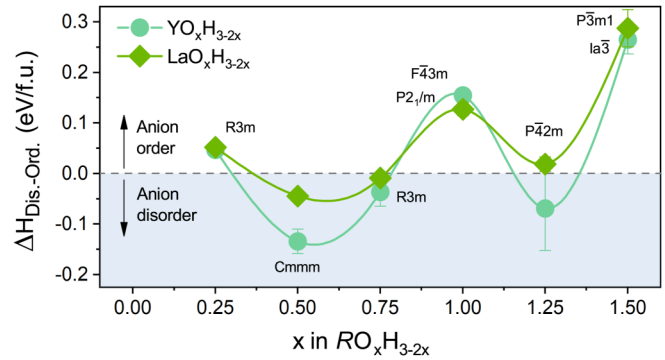

FIG. 3. Energy difference along the RO_xH_{3-2x} (R = Y, La) composition line between the anion-disordered and the most stable anion-ordered structure among those considered in this paper. For each composition, the space group of the most stable anion-ordered structure is indicated next to the point.

II. RESULTS

A. Energy

In this section we discuss the energy [38], after relaxation, of all structures considered in this paper. First, we show that anion-disorder does not lead to a large energy penalty compared to the anion-ordered polymorphs, but, in fact, within the group of structures considered in this paper, is even favourable for $0.25 < x < 1$. Second, we discuss the progressive stabilization (i.e., decrease of energy) upon increasing O:H content, rationalizing this trend in terms of lattice energy. Finally, we discuss the energy of all 1:1:1 *R*OH structures, and compare the computational results of this study to the many YOH and LaOH polymorphs reported in the literature.

Fukui *et al.* [9] have proposed that *R* oxyhydrides are stable in an anion-ordered structure only within a limited compositional interval around the 1:1:1 *R*OH composition. The results in Fig. 3 support this proposition, showing the energy difference between the anion-disordered structures and the most stable anion-ordered ones of same composition. At the 1:1:1 composition, we find an energy penalty for disorder of 0.16 eV/f.u. for YOH and 0.14 eV/f.u. for LaOH. In the H-rich region the trend inverts, and—among the structures considered in this paper—the anion-disordered ones present the lowest energy for compositions $x = 0.5$ and $x = 0.75$. For Y oxyhydrides, that is the case also in the O-rich region, at $x = 1.25$.

Figure 4(a) sketches the Born-Haber cycle of the oxyhydride, showing all contributions to its formation energy. The dependency of the formation energy upon the O:H ratio is shown for all structures in Figs. 4(b) (Y) and 4(c) (La). Here, the (negative) formation energy increases in magnitude upon increasing oxygen content, and—reflecting the ionic character of the oxyhydrides—it follows a trend that is almost identical for the two cations.

In an ionic compound, the lattice energy is in fact dominated by the crystal structure and by the oxidation state of the constituting ions, while their identity has a marginal influence. This is formalized in the Born-Landé equation [28]:

$$\Delta H_L = \frac{e^2}{4\pi\varepsilon_0} \sum_{i\neq j} \frac{z_i z_j}{|r_i - r_j|} \left(1 - \frac{1}{n}\right) \quad (2)$$

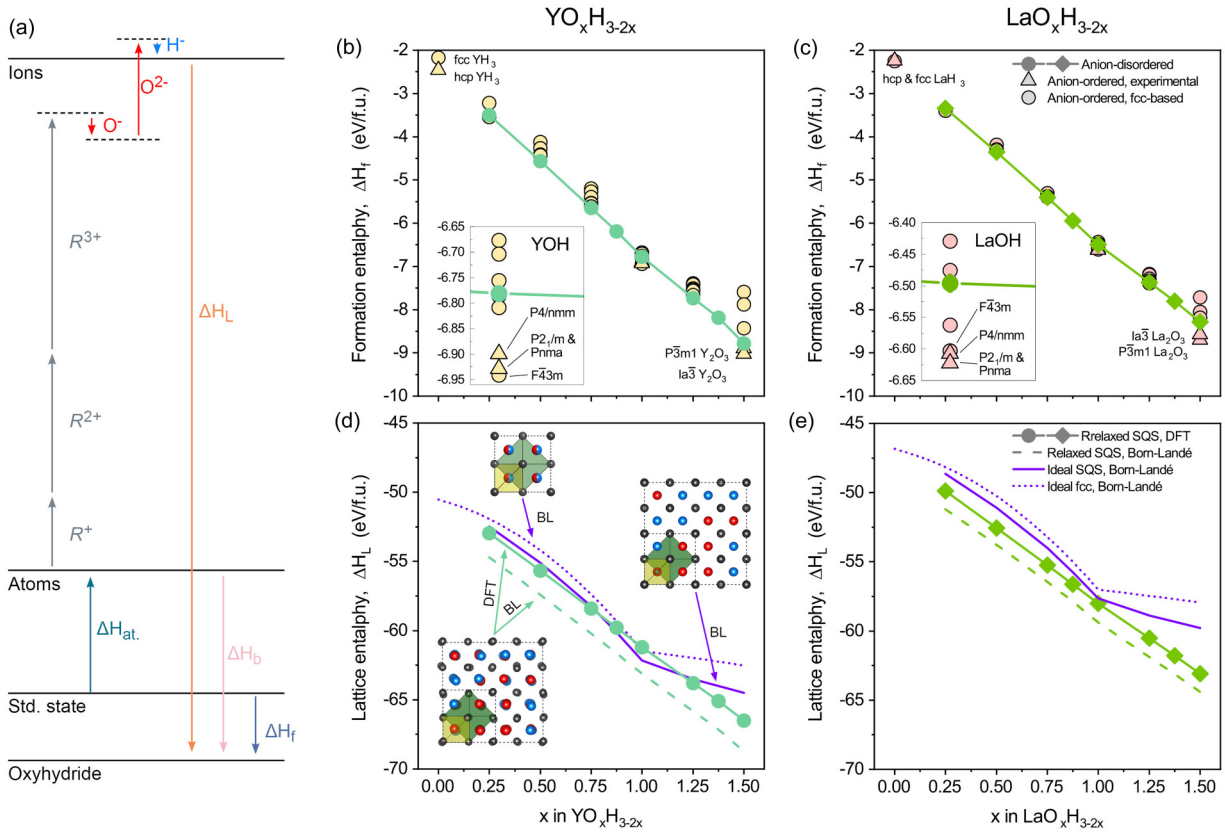

FIG. 4. (a) Born-Haber cycle of R oxyhydride. The arrows are at scale for the 1:1:1 composition and indicate: Atomization energy ($\Delta H_{\text{at.}}$), R ionization energies, O and H electron affinities, oxyhydride lattice energy (ΔH_L), binding energy (ΔH_b), and formation energy (ΔH_f). [(b), (c)] Influence of O:H ratio on the formation energy of Y and La oxyhydrides, respectively. The insets focus on the stoichiometric 1:1:1 composition. [(d), (e)] Influence of O:H ratio on the lattice energy of Y and La anion-disordered oxyhydrides, respectively. For $x \leqslant 1$, the (negative) lattice energy increases mainly due to a shift of charge from the less-stable octahedral to the more-stable tetrahedral anion sites. For $x > 1$, further stabilization results from a larger freedom for structural distortion related to the presence of empty tetrahedral sites. For comparison, the lattice energy evaluated with the Born-Landé equation is also reported for three different structural models of increasing resemblance to the real material: (i) idealized anion-disordered model based on $Fm\bar{3}m$ symmetry (dotted lines), (ii) nonrelaxed SQS structures (solid lines), and (iii) relaxed SQS structures (dashed lines).

where the i, j ions of oxidation state z are initially treated as point charges, and the resulting electrostatic energy (i.e., the Madelung energy) is subsequently corrected to account for an additional repulsion due to the finite atomic size. The identity of the ions therefore only enters in the mean Born-Landé exponent (n), which for the oxyhydrides we estimate as the weighted average of generalized Pauling's values ($n_Y \sim n_{Kr} = 10$, $n_{La} \sim n_{Xe} = 10$, $n_O \sim n_{Ne} = 7$, $n_H \sim n_{He} = 5$) [28]:

$$n = \frac{n_R + x n_O + (3-2x) n_H}{1 + x + (3-2x)}. \tag{3}$$

The lattice energy extracted from DFT of the anion-disordered Y and La oxyhydrides is reported as solid points in Figs. 4(d) and 4(e), respectively. This energy decreases upon increasing O:H ratio, with a slope that is very similar for both Y and La oxyhydrides due to the dominance of the Madelung term over the Born-Landé correction (see Fig. S5 in the SM [17]). The absolute values, instead, differ because of the different lattice parameters of Y and La oxyhydrides. Indeed, along the whole $R\text{O}_x\text{H}_{3-2x}$ composition line, we find a constant ratio $\Delta H_Y / \Delta H_{La} \sim 1.07(1)$ from DFT, in excellent agreement with the inverse ratio between lattice constants $a_{La}/a_Y \sim 1.07(1)$, and therefore in line with the $\Delta H_L \propto 1/r$ dependency expected from the Born-Landé equation.

To understand the origin of the progressive energy decrease upon increasing O:H ratio, an analysis of the Madelung energy is needed. A simplified discussion on the trend of Madelung energy along the $R\text{O}_x\text{H}_{3-2x}$ oxyhydride line can be found in our previous paper [13]. There, two compositional intervals of different behavior are identified under the approximation of an invariant fcc cation lattice and the assumption of idealized anion sites of average valence (e.g., in ROH, all tetrahedral anion sites are equivalently occupied by a point charge of –1.5 e). In the first interval ($x \leqslant 1$), the Madelung energy decreases monotonously due to an effective displacement of charge from the octahedral anion sites towards the more stable tetrahedral sites, leading on average to a shorter distance between positive and negative charges. In the second interval ($x > 1$), no charge displacement occurs and the Madelung energy levels off. This model, after correction with

the Born-Landé factor [purple-dotted lines in Figs. 4(d) and 4(e)], matches well the lattice energies extracted from DFT in the interval $x \leqslant 1$. It does not account, however, for the further decrease in lattice energy that occurs in the second interval ($x > 1$). We exclude that the plateau at $x > 1$ is an artefact due to the assumption of an average valency of the anion sites, because a comparable plateau is found evaluating the lattice energy of ideal (i.e., nonrelaxed) SQS structures with the Born-Landé equation (purple-solid lines). In contrast, when the Born-Landé equation is used for the relaxed SQS structures, we find an excellent agreement with the slope of the lattice energy as obtained by DFT. This again verifies the ionic character of the oxyhydrides, and shows that the further energy decrease that occurs for $x > 1$ is the result of structural distortions—prominent in the O-rich interval—that lead to more stable atomic configurations.

Clearly, the freedom for structural distortions correlates with the presence of empty tetrahedral sites, which are fully occupied for $x \leqslant 1$, but progressively deplete for $x > 1$. It is therefore not surprising that the Y_2O_3 oxide crystallizes in the $I\bar{3}a$-bixbyite structure, as this is a cubic superstructure where the tetrahedral empty sites order to maximize (minimize) distortion (repulsion) [39]. We find the bixbyite structure to be in fact ∼0.3 eV/f.u. lower in energy compared to the disordered counterpart. In analogy, it is expected that at 0 K other anion-ordered oxyhydride structures of lower energy could be found considering ordering schemes that extend beyond the first coordination shell. However, with increasing temperature, the additional effect of configurational entropy will further stabilize the disordered limit. At the time of writing, it remains unclear if it is configurational entropy, rather than kinetic limitations during the material synthesis, the reason why no anion-ordered polymorphs have been experimentally reported outside the 1:1:1 *R*OH composition and the binary RH_3 and R_2O_3 extremes.

In terms of relative stability of crystal structures, clear differences between Y and La compounds are found at the binary extremes, which are well known to form different thermodynamically stable phases (namely, $P6_3/mmc$-YH_3 vs $Fm\bar{3}m$-LaH_3, and $I\bar{3}a$-Y_2O_3 vs $P\bar{3}m1$-La_2O_3) [39], and at the 1:1:1 composition [Figs. 4(b) and 4(c), insets]. In the case of the 1:1:1 composition, the energy difference between the three known anion-ordered structures ($P4/nmm$, $Pnma$, and $P2_1/m$) is relatively small, explaining why different polymorphs have been reported on different occasions. This includes $Pnma$ [10] and $P2_1/m$ [9] for YOH, and $P4/nmm$ [1,12,40] and $P2_1/m$ [9] for LaOH. Notably, the $F\bar{4}3m$ phase has never been reported for YOH, which is particularly surprising as we predict it to be the energetically most favourable structure. This result is in agreement with a previous paper, where, in addition to an identical theoretical conclusion for Y, it was experimentally shown that other small *R*s (Dy, Ho, Er) do form $F\bar{4}3m$-*R*OH [42]. Since the anions alternate within its lattice, the $F\bar{4}3m$ phase is the one that effectively maximizes the distance between O^{2-} ions, and consequently minimizes the overall electrostatic repulsion in the anion sublattice; therefore, one intuitively expects it to be particularly favourable for the smaller *R*s.

Despite the higher energy, anion-disordered *R*OH have been reported in a multitude of cases for the smaller *R* cations [8,9,12,40], as well as for LaOH synthesized at high pressure [9]. Since the synthesis of oxyhydride powders relies on a high-temperature solid state reaction between RH_3 and R_2O_3, we suppose that kinetic limitations, together with configurational entropy, lead to the resulting anion-disordered phase. We stress, however, that XRD alone is not sufficient to discriminate between the anion-disordered phase and the anion-ordered $F\bar{4}3m$ polymorph, and care should be taken in the absence of neutron diffraction data (e.g., in case of Refs. [9,40]).

B. Compositional limits of the anion-disordered phase

Relaxing the generated SQS gives an indication of their metastability;[41] if the atoms change site or restructure beyond small distortions, it indicates that the hypothesised structure was not metastable. We exploit this fact to computationally verify the results of Fukui *et al.* [9], who recently proposed that the compositional interval in which the anion-disordered phase is stable depends on the size of the cation, with La and Y being two extremes. It is worth mentioning that structural relaxation does not sample the whole space of parameters, but rather finds a local minimum not too far from the starting positions. This approach is, thus, incapable of predicting long-range anion reordering or phase segregations, but is nevertheless suitable to discuss the maximum range of O:H ratios in which the anion-disordered CaF_2-type phase is metastable.

The radial pair distribution function (PDF) and its cumulative value (CPDF) are the most transparent indicators to assess the type and the extent of the structural rearrangement that the disordered structures undergo during relaxation. Irrespective of the composition, we find that the R^{3+} and O^{2-} ions do not move significantly from their original site (see Fig. S6 in the SM [17]). For the H sublattice the case is different, and a change in symmetry occurs depending on the cation and on the O:H ratio (Fig. 5 and Fig. S7 in the SM [17]). In the following, we first discuss the O-rich compositional interval, and then the H-rich one.

In the O-rich interval ($x > 1$), both O^{2-} and H^- anions occupy exclusively the tetrahedral sites of the cation lattice, which are the energetically most stable in this compositional range [13]. As such, there is no driving force to induce local rearrangements beyond small distortions. In Fig. 5 one observes one broad peak corresponding to the tetrahedral H^-, whose spread is due to small distortions and whose overlaying features are the result of the finite number of possible local environments.

In the H-rich compositional range ($x < 1$), where all tetrahedral sites and part of the octahedral ones are occupied, the electrostatic repulsion between neighboring anions becomes more determining [9]. The associated electrostatic energy scales as $1/r$, and is thus stronger for smaller lattice constants. The H sublattice of the most H-rich Y oxyhydrides ($x \leqslant 0.5$) appears in fact destabilized, as indicated in Fig. 5 by the appearance of two new coordination shells at ∼3.2 Å and ∼3.7 Å. These features do not match the initial symmetry, but rather correspond to the second and third coordination shells that result from a single highly distorted octahedral H^- site. Conversely, the bigger La oxyhydrides maintain the

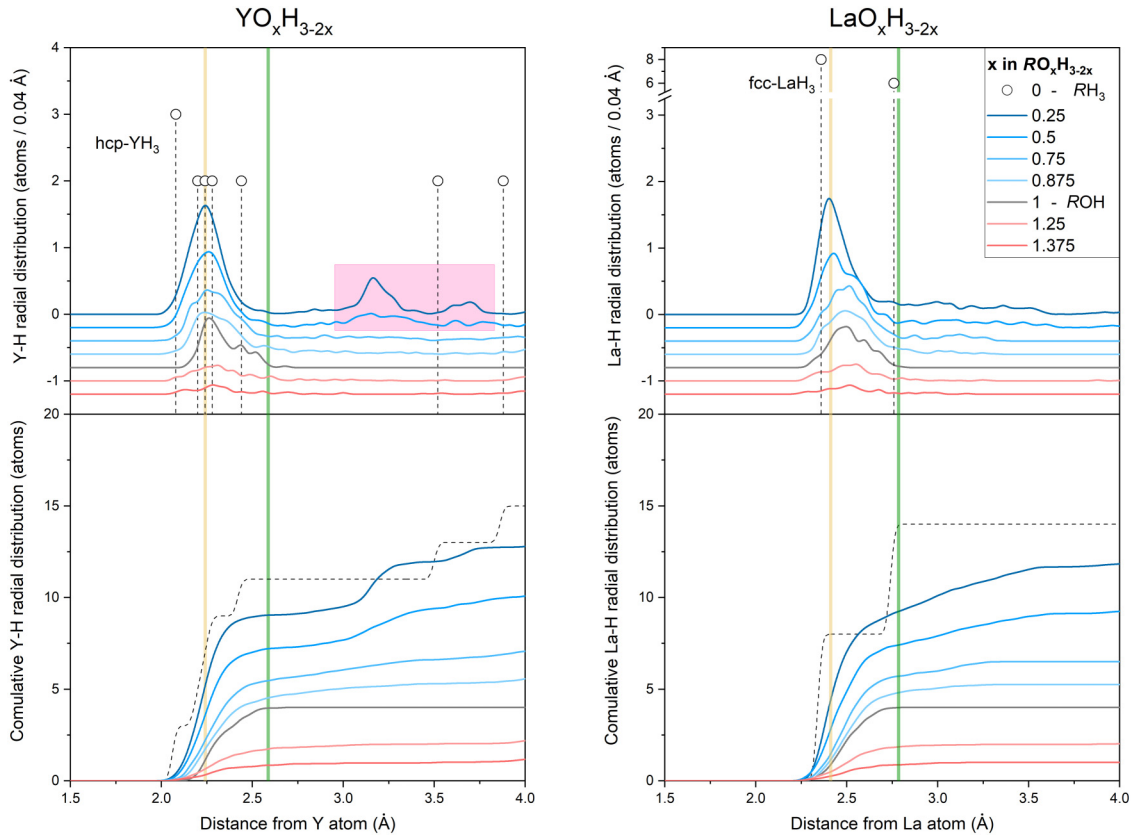

FIG. 5. R−H radial pair distribution functions (top panels) and their cumulative values (bottom panels) for the relaxed SQS of Y and La anion-disordered oxyhydrides. The dashed-vertical lines refer to the thermodynamically stable $P6_3/mmc$-YH_3 and $Fm\bar{3}m$-LaH_3 hydrides. Yellow and green vertical lines mark the position of tetrahedral and octahedral interstitial sites for an ideal fcc structure with lattice constant tuned to match the $RO_{0.25}H_{2.5}$ composition. The pink region highlights peaks that do not match the CaF_2-type structure. To help visualization, lines in the top panels are shifted downward by a constant value of −0.2.

CaF_2-type structure throughout the whole compositional interval, although with a significant degree of distortion. The anion repulsion close by an O^{2-} ion, in particular, leads to the displacement of the neighboring octahedral H^- and therefore to the broadening of the corresponding peak (step) in the PDF (CPDF). The different behavior between Y and La oxyhydrides aligns with the different thermodynamically stable phases of the Y and La trihydrides, which is hexagonal for YH_3 and cubic for LaH_3.

Figure 6 gives a visual impression of the structural rearrangements that occur upon relaxation of an anion-disordered H-rich (x = 0.25) oxyhydride. In the case of Y, the proximity of a tetrahedral H^- to several octahedral H^- is energetically unfavourable, therefore it is advantageous for the tetrahedral H^- to shift towards an empty octahedral position. After that, all the octahedral H^- relax towards the empty tetrahedral site. An approximated description in terms of tetrahedral and octahedral anion sites is no longer valid as all H^- ions now sit in comparable intermediate positions. This reorganization reflects the propensity to deform towards a hexagonal YH_3-like structure, a tendency likely present also for higher oxygen contents but that becomes evident in the PDF (CPDF) only for $x \leqslant 0.5$. In the case of La, no major reorganization happens and the ions only relax within the space of their initial site.

In view of the symmetry change of the H sublattice, we conclude that the interval of metastability of anion-disordered Y oxyhydrides based on the CaF_2-type structure is limited to $x > 0.5$. On the contrary, anion-disordered La oxyhydrides

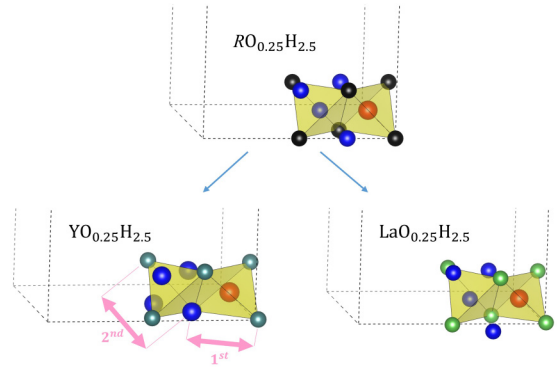

FIG. 6. Example of the effect of structural relaxation on the anion-disordered structure of $YO_{0.25}H_{2.5}$ and $LaO_{0.25}H_{2.5}$ oxyhydrides. The yellow polygons indicate the tetrahedral anion sites. Irrespective of the composition, the displacement of R^{3+} and O^{2-} is minimal. However, a shift of the tetrahedral H^- to the empty octahedral sites is observable in the case of Y (see text). The pink arrows indicate the interatomic distances that correspond to the two additional peaks in the PDF (Fig. 5). In the case of La, no major reorganization happens and the ions only relax within the space of their initial site.

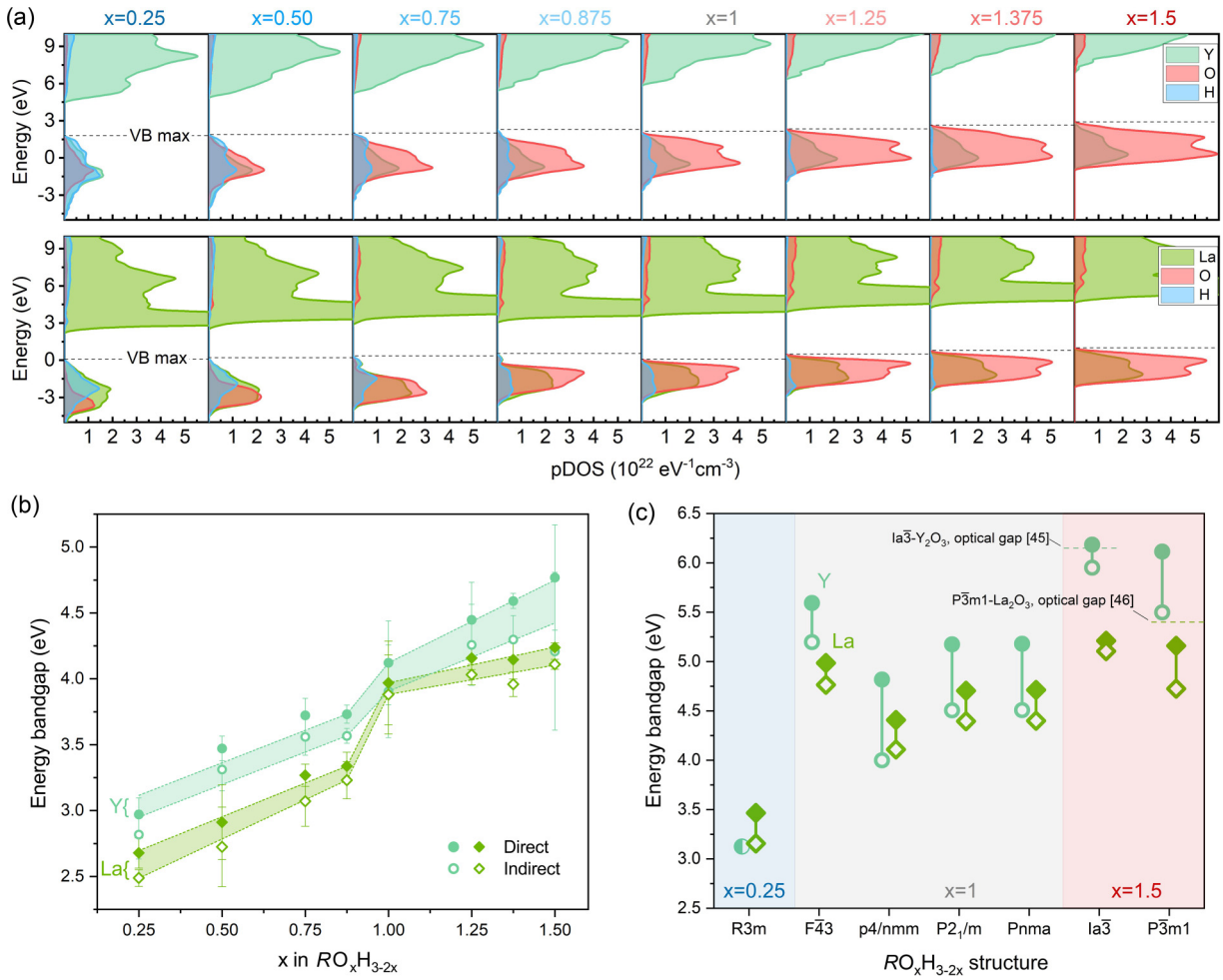

FIG. 7. (a) Projected mBJ density of states around the Fermi level for Y and La anion-disordered RO_xH_{3-2x} oxyhydrides. The valence band has hybrid character, with the extend of the hybridization depending on the lattice dimension and on the rearrangements of the H sublattice involving tetrahedral and octahedral sites (see text). A Gaussian smearing of 0.2 eV has been used in the figure to aid visualization. (b) Dependency of the direct and indirect energy band gaps upon the O:H ratio in Y and La anion-disordered RO_xH_{3-2x} oxyhydrides. The energy band gap widens upon increasing O:H content, with a bigger jump at $x \geqslant 1$, where the octahedral anion sites are all empty. Lines are a guide for the eyes. (c) Direct/Indirect band gaps (filled/open points) of the Y and La anion-ordered oxyhydrides of lower energy compared to the anion-disordered phase. Reference values for the optical gap of R_2O_3 oxides (corresponding to $x = 1.5$) are also reported, showing the excellent predictive ability of the mBJ scheme ($\delta E_g < 10\%$).

appear metastable along the whole $RH_3 - R_2O_3$ composition line.

The fact that (i) different SQS of same composition relax towards comparable pair radial distributions, and (ii) that the different behavior shown by Y and La compounds is in excellent agreement with the experimental work of Fukui *et al.* [9] indicates that the finite size of the SQS does not introduce artefacts that overrule the structural behavior of the two different materials.

C. Optical properties

Following from the valence implied by the oxyhydride composition ($R^{3+}O_x^{2-}H_{3-2x}^{-}$), and the large difference in Pauling electronegativity between cations ($Y = 1.22$, $La = 1.1$) and anions ($O = 3.44$, $H = 2.20$), all compounds simulated in this paper show a sizable energy band gap (E_g) between the valence band (VB), dominated by occupied anion states, and the conduction band (CB), largely made of empty cation states.

Figure 7(a) reports the pDOS of Y and La anion-disordered oxyhydrides around the Fermi level. The pDOS from –25 eV to +25 eV is reported in Fig. S8 in the SM [17]. Most interestingly, across the whole RO_xH_{3-2x} composition line, the valence band retains a hybrid character, which originates from the overlap of Y (La) 5s4d (6s5d), O 2p, and H 1s atomic orbitals. In the H-rich range ($x < 1$), however, the extent of the hybridization between O 2p and H 1s orbitals is different among Y and La compounds: In Y oxyhydrides, O and H states overlap thoroughly, while for La oxyhydrides the top of the valence band is largely dominated by H states. Likely, the rearrangement of the H sublattice that occurs in Y oxyhydrides for $x \leqslant 0.5$ contributes to the strong hybridization observed here, since there is no more distinction between tetrahedral and octahedral H. Conversely, in La oxyhydrides, the distinct tetrahedral and octahedral hydride ions contribute

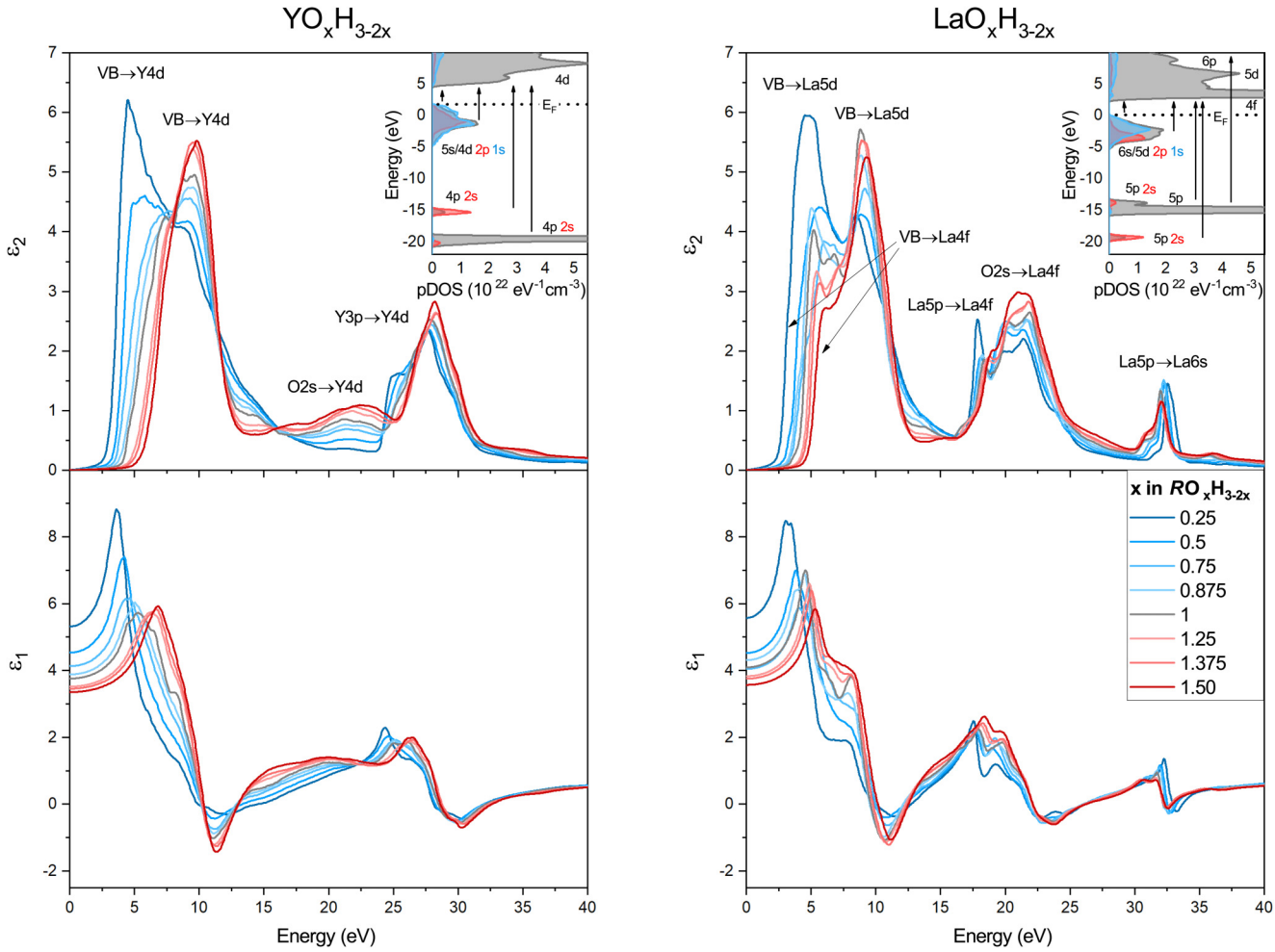

FIG. 8. Imaginary and real mBJ dielectric functions of Y and La anion-ordered RO_xH_{3-2x} oxyhydrides upon increasing O:H content. The electronic transitions responsible for the main features are indicated in the insets, which report the pDOS of $YO_{0.25}H_{2.5}$ and $LaO_{0.25}H_{2.5}$, respectively.

differently to the DOS, with the less-stable octahedral H^- resulting in states of higher energy, that in fact disappear at higher O:H ratios. Additionally, the larger interatomic distances in La oxyhydrides imply a reduced overlap between H and O atomic orbitals, leading to a weaker hybridization and, in general, to narrower energy bands compared to Y oxyhydrides of the same O:H ratio.

For both Y and La anion-disordered oxyhydrides, the resulting energy band gaps are reported in Fig. 7(b). Here, direct and indirect band gaps are shown, their difference is rather small in view of the limited periodicity of the disordered anion sublattice. For both cations, the band gap widens upon increasing the O:H ratio, with a bigger step at $x = 1$ that further confirms how the octahedral H is largely responsible for the topmost part of the VB. For all O:H ratios, we find that the band gap of La oxyhydrides is smaller than that of Y oxyhydrides, a consequence of the additional La 4f unoccupied states that form the the bottom of the CB. A similar trend of band gap expansions, and smaller energy band gaps for La compared to Y, is generally observed for the anion-ordered polymorphs as well [Fig. 7(c)].

Experimental optical gaps are available for the ordered, binary extremes of the RH_3-R_2O_3 composition line, which are here used to further validate the accuracy of the mBJ scheme. The RH_3 trihydrides pose a notorious challenge to most flavours of DFT, with LDA/GGA approximations erroneously predicting semimetallic character and self-consistent *GW* calculations returning a severely underestimated band gap [43]. While an exact description of the RH_3 is beyond the scope of this paper, in Fig. S4 in the SM [17] we show that the mBJ scheme successfully predicts the semiconducting character of YH_3 (optical gap 2.5 e.V.) [44] with a quantitative estimation (∼1 e.V.) in line with previous *GW* studies [43]. Concerning the R_2O_3 oxides, we find an excellent match within 0.1 eV and 0.3 eV between the direct bandgaps computed with the mBJ scheme and the experimental optical gaps of $Ia\bar{3}$-Y_2O_3 (6.15 eV) [45] and $P\bar{3}m1$-La_2O_3 (5.5 eV) [46], respectively.

The prominent role of octahedral H in determining the RO_xH_{3-2x} optical behavior is even clearer from the evolution of the dielectric function upon increasing O:H ratio (Fig. 8). The imaginary part (ε_2), reported in the top panels, shows a main feature between 3 eV and 10 eV. This corresponds to the electronic transitions from VB to CB, with an onset closely matching the direct band gap of the compounds, and two peaks which can be connected to the octahedral and

tetrahedral anions. In fact, the first (second) peak decreases (increases) upon increasing O:H ratio, with x = 1 marking, again, a transition point for properties dependent on the anion composition. Here, the ratio between the two peaks inverts. The first peak disappears completely in the case of Y, whose oxyhydrides have a smoother dielectric function because fewer electronic transitions are possible, and their energy bands are wider and more spaced compared to the case of La. In the case of La, the sharp 4f-band at the CB bottom contributes to the persistence of a two-peak structure.

A related trend upon O:H content can be seen in the real part of the dielectric function. The refractive behavior at UV-VIS-NIR frequencies is defined by the first ∼5 eV, where $R\mathrm{O_xH_{3-2x}}$ oxyhydrides of higher H content show significantly higher ε_1.

III. DISCUSSION

Disorder-order transition in *R* oxyhydride thin films

At the time of writing, there are no experimental data on the optical properties of either anion-ordered or anion-disordered $R\mathrm{O_xH_{3-2x}}$ produced via the conventional solid-state reaction between $R\mathrm{H_3}$ and $R_2\mathrm{O_3}$ precursors. However, the optical properties of *R* oxyhydride films produced via post-oxidation of reactively sputtered $R\mathrm{H_2}$ films have been studied extensively, with a particular focus on their reversible photochromism. Such photochromic effect has been so far reported for a variety or *R* cations (*R* = Sc, Y, Nd, Gd, Dy, Er) [3,47–49], and in a range of O:H ratios as big as $0.5 < x < 1.3$ [3].

While the composition of the oxyhydride and the deposition conditions influence the extent and the speed of photochromism [4], the general presence of the phenomenon indicates that its origin is intrinsic to the *R* oxyhydride thin film material. Currently, there is not yet conclusive agreement concerning (i) the nature of the absorbing species responsible for the photodarkening, (ii) the mechanism of their formation under illumination and subsequent disappearance during bleaching in the dark, and (iii) the driving forces behind these processes. While the photodarkening is initiated by an interband electronic transition, most research converges towards the idea that structural rearrangements enabled by the high H (local)mobility are at the heart of the photochromism. In this sense, it was hinted that the photodarkening depends on the segregation of an absorbing phase [15,16], a process accompanied by reversible contraction of the crystal lattice [50], and quenching of the NMR signal of the most mobile H fraction (∼3%) [51]. A reversible change in the H sublattice upon illumination was recently suggested as well via muon spin rotation spectroscopy (μSR) [52]. Finally, the bleaching was shown to be a thermally activated process [53].

In this context, a deeper understanding of the crystal structure and anion sublattice of the sputtered $R\mathrm{O_xH_{3-2x}}$ is important to further explore the photo-induced process, as well as to assess the actual similarity to the well-characterized oxyhydride powders. Since neutron diffraction is not a viable option for thin films, as per today there is no experimental information on their anion sublattice other than the already discussed preference for the tetrahedral sites [13]. Considering that the oxidation of the parent $R\mathrm{H_2}$ occurs at room temperature and rapidly, thus likely missing the narrow energetic minima expected for anion-ordered structures, a model based on anion-disorder was heuristically proposed for the photochromic $R\mathrm{O_xH_{3-2x}}$ thin films.[3,13] In fact, independently from cation and O:H ratio, the fcc symmetry was generally reported for the cation sublattice, with XRD patterns lacking any additional superstructure peaks typical of anion ordering (e.g., due to periodicity in the small distortion as in the $Ia\bar{3}$ oxide) [3,13,49]. The hypothesis of an anion-disordered structure can now be investigated by comparing the optical properties computed in this paper with the experimental ones of $\mathrm{YO_xH_{3-2x}}$ thin films.

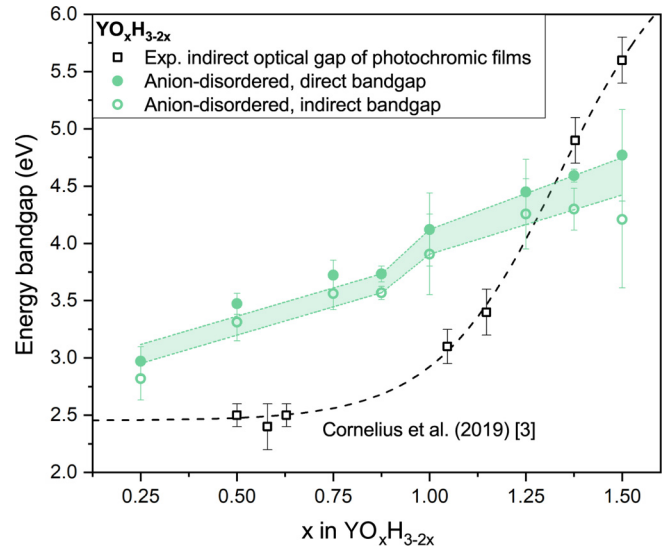

FIG. 9. Comparison between the experimental optical gap of photochromic Y oxyhydride thin films [3] and the direct/indirect energy band gaps computed for anion-disordered $\mathrm{YO_xH_{3-2x}}$. Lines are a guide for the eyes.

Figure 9 shows the comparison between computed energy bandgaps and the indirect optical gap from Cornelius *et al.* [3]. The anion-disordered model captures a trend of increasing gap for increasing O:H ratio, however, up to $x \leqslant 1$, the computed band gaps systematically overestimate the experimental ones by 0.5–1 eV. This is a significant difference even considering that excitonic effects were neglected. Comparison to the reference compounds $R\mathrm{H_3}$ and $R_2\mathrm{O_3}$ suggests the absence of systematic overestimations of the band gaps in our simulations; $R\mathrm{H_3}$ trihydrides are in fact known to present the opposite challenge to any flavour of DFT (including mBJ, see Fig. S4 in the SM [17]) [43], while the optical gaps of the $R_2\mathrm{O_3}$ match our results within 0.3 eV.

It is worth noting that all anion-ordered structures return even higher bandgaps and do not show a monotonously increasing trend with O:H ratio (Fig. 7 c and Fig. S9 in the SM [17]), therefore, despite the disagreement we observe with the experiment, anion-disorder remains the best candidate for the anion sublattice of the H-rich (i.e., $x \leqslant 1$) Y oxyhydride thin films. Two aspects not included in the model might be responsible for the mismatch with the experimental optical gaps, namely: (i) unaccounted defects that might give in-gap states and, (ii) the substrate-induced stress and the limited freedom for distortion of the grains in the polycrystalline films. In

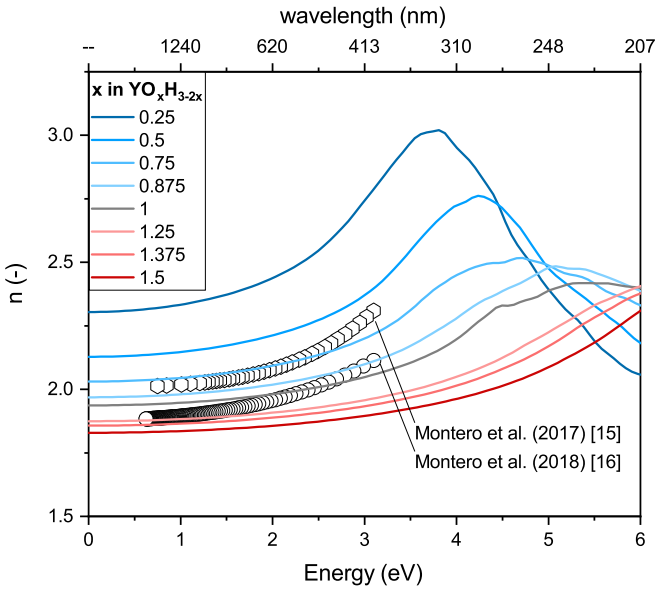

FIG. 10. Comparison between the experimental refractive index of photochromic Y oxyhydride thin films [15,16] and the ones computed for anion-disordered YO_xH_{3-2x}.

addition, (iii) it is possible that compositional inhomogeneity within the sputtered films results in band extrema that do not reflect the average RO_xH_{3-2x} composition, but rather some local deviations, e.g., a very H-rich region more similar to YH_3 ($E_g \sim 2.6$ eV).

Being less sensitive to defects and local inhomogeneity (at least in the absence of absorption, for $E \ll E_g$), the refractive index ($\tilde{n} = n + ik = \varepsilon^{1/2}$) would be a better property to compare. However, in the limit of $E \ll E_g$, it is the composition and not the crystal structure that dominates its value (see Fig. S10 in the SM [17]). Focusing on the energies relevant to UV-VIS-nIR spectroscopy, Fig. 10 shows the good agreement between the computed refractive index of anion-disordered YO_xH_{3-2x} and reported experimental values [15,16], further proving that the oxyhydride RO_xH_{3-2x} composition well describes the photochromic thin films. Unfortunately the exact O:H ratio of the films films measured in Refs. [15,16] was not known. However their refractive indexes match the values computed for the interval x : [0.75, 1.25], which—considering the challenges of predicting optical properties *ab initio*—is largely compatible with the composition range of x : [0.5, 1] that is expected for air-oxidized thin films [4].

We conclude, that an anion-disordered sublattice is the most likely configuration for H-rich photochromic thin films ($x < 1$). The situation appears different for O-rich compositions ($x > 1$), where the experimental optical gaps show a steep increase, which is not present in the trend computed for the anion-disordered oxyhydrides. This suggest that a certain degree of anion ordering must be present in O-rich oxyhydrides films, intuitively facilitated by the presence of empty tetrahedral sites. Notably, reactively sputtered Y_2O_3 films assume the bixbyite $Ia\bar{3}$ phase, and their experimental optical gap of 5.7 eV matches well both reference and computed values. A somewhat gradual transition from anion-disorder to anion-order is thus expected for $x > 1$.

IV. CONCLUSIONS

In this paper, we have introduced a set of special quasirandom structures (SQS) to model the anion-disordered lattice of RO_xH_{3-2x} oxyhydrides along the entire $RH_3 - R_2O_3$ composition line. This allowed us to investigate *ab initio* the influence of the O:H ratio of the energy, metastability, and optical properties of Y and La oxyhydrides.

In agreement with the experimental result of Fukui *et al.* [9], anion-ordered polymorphs ($P4/nmm$, $Pnma$, and $P2_1/m$) are energetically favoured for the ROH 1:1:1 stoichiometric oxyhydrides. Notably, we find that the energetically most stable YOH has $F\bar{4}3m$ symmetry, a so-far experimentally unreported structure where the Y^{3+} cations assume fcc lattice and the H^- and O^{2-} anions alternate in its tetrahedral interstitial sites. Comparing to the most stable anion-ordered polymorphs among those considered in this paper, anion-disorder leads to an energy penalty of 0.16 eV/f.u. and 0.14 eV/f.u. for YOH and LaOH, respectively. Moving away from the 1:1:1 composition, the energy penalty becomes lower, and the anion-disordered phase even presents the lowest energy in the H-rich composition interval for both Y and La oxyhydrides.

Upon increasing oxygen content, anion-disordered RO_xH_{3-2x} show a progressive stabilization, which we rationalize in terms of increasing (negative) lattice energy. For $x \leqslant 1$, this is due to a shift of charge from the octahedral to the more-stable tetrahedral anion sites. For $x > 1$, further stabilization results from a larger freedom for structural distortion related to the presence of empty tetrahedral sites.

We find that the cation size (and thus the lattice constant) determines the compositional interval in which the CaF_2-type anion-disordered phase is metastable against spontaneous structural rearrangement of the anion sublattice. In particular, the bigger cell of La oxyhydride can accommodate any O:H ratios, while the most H-rich ($x \leqslant 0.5$) anion-disordered Y oxyhydrides proved unstable.

Finally, the influence of the O:H ratio on the electronic band gap, DOS, and dielectric function of anion-disordered oxyhydrides was discussed. To do so, in our simulation we employed—and validated—the mBJ scheme, achieving an accuracy comparable to far more expensive *GW* methods. Our results show major differences between H-rich and O-rich regimes. For $x < 1$, we find that the octahedral H^- anions play a decisive role: they form electronic states at the top of the valence band, which reduce the energy band gap and dominate the electronic transitions at lower energies, thus increasing the refractive index of the material in the VIS-nIR spectral range.

A comparison of these results to the experimental data available for photochromic Y oxyhydride thin films reinforces the hypothesis of anion-disorder for H-rich oxyhydrides ($x < 1$), while it hints towards some degree of anion ordering for the O-rich ones ($x > 1$).

ACKNOWLEDGMENTS

The authors thank Dr. Steffen Cornelius and Herman Schreuders for the insightful conversations; and Dr. José Montero for sharing experimental data of refractive index.

This work was partially supported by the Mat4Sus research program with Project No. 680.M4SF.034 and by the Open Technology research program with Project No. 13282; both financed by the Dutch Research Council (NWO).

[1] K. Fukui, S. Iimura, T. Tada, S. Fujitsu, M. Sasase, H. Tamatsukuri, T. Honda, K. Ikeda, T. Otomo, and H. Hosono, Characteristic fast H^- ion conduction in oxygen-substituted lanthanum hydride, Nat. Commun. **10**, 2578 (2019).

[2] T. Mongstad, C. Platzer-Björkman, J. P. Maehlen, L. P. Mooij, Y. Pivak, B. Dam, E. S. Marstein, B. C. Hauback, and S. Z. Karazhanov, A new thin film photochromic material: Oxygen-containing yttrium hydride, Sol. Energy Mater. Sol. Cells **95**, 3596 (2011).

[3] S. Cornelius, G. Colombi, F. Nafezarefi, H. Schreuders, R. Heller, F. Munnik, and B. Dam, Oxyhydride nature of rare-earth-based photochromic thin films, J. Phys. Chem. Lett. **10**, 1342 (2019).

[4] G. Colombi, T. De Krom, D. Chaykina, S. Cornelius, S. W. H. Eijt, and B. Dam, Influence of cation (R = Sc, Y, Gd) and O/H anion ratio on the photochromic properties of RO_xH_{32x} thin films, ACS Photonics **8**, 709 (2021).

[5] G. Kobayashi, Y. Hinuma, S. Matsuoka, A. Watanabe, M. Iqbal, M. Hirayama, M. Yonemura, T. Kamiyama, I. Tanaka, and R. Kanno, Pure H^- conduction in oxyhydrides, Science **351**, 1314 (2016).

[6] H. Kageyama, K. Hayashi, K. Maeda, J. P. Attfield, Z. Hiroi, J. M. Rondinelli, and K. R. Poeppelmeier, Expanding frontiers in materials chemistry and physics with multiple anions, Nat. Commun. **9**, 772 (2018).

[7] Y. Kobayashi, O. Hernandez, C. Tassel, and H. Kageyama, New chemistry of transition metal oxyhydrides, Sci. Technol. Adv. Mater. **18**, 905 (2017).

[8] T. Broux, H. Ubukata, C. J. Pickard, F. Takeiri, G. Kobayashi, S. Kawaguchi, M. Yonemura, Y. Goto, C. Tassel, and H. Kageyama, High-pressure polymorphs of LaHO with anion coordination, J. Am. Chem. Soc. **141**, 8717 (2019).

[9] K. Fukui, S. Iimura, J. Wang, T. Tada, T. Honda, K. Ikeda, T. Otomo, and H. Hosono, Stabilization factor of anion-excess fluorite phase for fast anion conduction, Chem. Mater. **33**, 1867 (2021).

[10] N. Zapp, H. Auer, and H. Kohlmann, YHO, an air-stable ionic hydride, Inorg. Chem. **58**, 14635 (2019).

[11] N. Zapp, D. Sheptyakov, A. Franz, and H. Kohlmann, HoHO: A paramagnetic air-resistant ionic hydride with ordered anions, Inorg. Chem. **60**, 3972 (2021).

[12] H. Ubukata, T. Broux, F. Takeiri, K. Shitara, H. Yamashita, A. Kuwabara, G. Kobayashi, and H. Kageyama, Hydride conductivity in an anion-ordered fluorite structure LnHO with an enlarged bottleneck, Chem. Mater. **31**, 7360 (2019).

[13] G. Colombi, S. Cornelius, A. Longo, and B. Dam, Structure model for anion-disordered photochromic gadolinium oxyhydride thin films, J. Phys. Chem. C **124**, 13541 (2020).

[14] K. Ooya, J. Li, K. Fukui, S. Iimura, T. Nakao, K. Ogasawara, M. Sasase, H. Abe, Y. Niwa, M. Kitano, and H. Hosono, Ruthenium catalysts promoted by lanthanide oxyhydrides with high hydride-ion mobility for low-temperature ammonia synthesis, Adv. Energy Mater. **11**, 2003723 (2021).

[15] J. Montero, F. A. Martinsen, M. García-Tecedor, S. Z. Karazhanov, D. Maestre, B. Hauback, and E. S. Marstein, Photochromic mechanism in oxygen-containing yttrium hydride thin films: An optical perspective, Phys. Rev. B **95**, 201301(R) (2017).

[16] J. Montero and S. Z. Karazhanov, Spectroscopic ellipsometry and microstructure characterization of photochromic oxygen-containing yttrium hydride thin films, Phys. Status Solidi A **215**, 1701039 (2018).

[17] See Supplemental Material at http://link.aps.org/supplemental/10.1103/PhysRevB.105.054208 for further computational details and validation, and additional information on the structural and electronic properties of anion-ordered and anion-disordered Y and La oxyhydrides. SQS structural models (VASP POSCAR files) available for download.

[18] A. Zunger, S.-H. Wei, L. G. Ferreira, and J. E. Bernard, Special Quasirandom Structures, Phys. Rev. Lett. **65**, 353 (1990).

[19] A. van de Walle, P. Tiwary, M. M. de Jong, D. L. Olmsted, M. D. Asta, A. Dick, D. Shin, Y. Wang, L.-Q. Chen, and Z.-K. Liu, Efficient stochastic generation of special quasirandom structures, Calphad **42**, 13 (2013).

[20] A. van de Walle, M. D. Asta, and G. Ceder, The alloy theoretic automated toolkit: A user guide, Calphad **26**, 539 (2002).

[21] G. Kresse and J. Furthmüller, Efficient iterative schemes for *ab initio* total-energy calculations using a plane-wave basis set, Phys. Rev. B **54**, 11169 (1996).

[22] G. Kresse and J. Furthmüller, Efficiency of *ab-initio* total energy calculations for metals and semiconductors using a plane-wave basis set, Comput. Mater. Sci. **6**, 15 (1996).

[23] P. E. Blöchl, Projector augmented-wave method, Phys. Rev. B **50**, 17953 (1994).

[24] G. Kresse and D. Joubert, From ultrasoft pseudopotentials to the projector augmented-wave method, Phys. Rev. B **59**, 1758 (1999).

[25] J. P. Perdew, K. Burke, and M. Ernzerhof, Generalized Gradient Approximation Made Simple, Phys. Rev. Lett. **77**, 3865 (1996).

[26] J. P. Perdew, K. Burke, and M. Ernzerhof, Generalized Gradient Approximation Made Simple [Phys. Rev. Lett. 77, 3865 (1996)], Phys. Rev. Lett. **78**, 1396(E) (1997).

[27] A. Kramida, Yu. Ralchenko, J. Reader, and NIST ASD Team, NIST Atomic Spectra Database (ver. 5.9), [Online]. Available: `https://physics.nist.gov/asd` [2021, November 1]. National Institute of Standards and Technology, Gaithersburg, MD. (2021).

[28] J. E. Huheey, E. A. Keiter, R. L. Keiter, and O. K. Medhi, *Inorganic Chemistry: Principles of Structure and Reactivity* (Springer, New York, 2006), pp. 99–104.

[29] K. Mommaand F. Izumi, VESTA 3 for three-dimensional visualization of crystal, volumetric and morphology data, J. Appl. Crystallogr. **44**, 1272 (2011).

[30] P. P. Ewald, Die berechnung optischer und elektrostatischer gitterpotentiale, Ann. Phys. (Leipzig) **369**, 253 (1921).

[31] A. D. Beckeand E. R. Johnson, A simple effective potential for exchange, J. Chem. Phys. **124**, 221101 (2006).

[32] F. Tranand P. Blaha, Accurate Band Gaps of Semiconductors and Insulators with a Semilocal Exchange-Correlation Potential, Phys. Rev. Lett. **102**, 226401 (2009).

[33] M. Shishkinand G. Kresse, Implementation and performance of the frequency-dependent GW method within the PAW framework, Phys. Rev. B **74**, 035101 (2006).

[34] M. Shishkinand G. Kresse, Self-consistent GW calculations for semiconductors and insulators, Phys. Rev. B **75**, 235102 (2007).

[35] M. Shishkin, M. Marsman, and G. Kresse, Accurate Quasiparticle Spectra from Self-Consistent GW Calculations with Vertex Corrections, Phys. Rev. Lett. **99**, 246403 (2007).

[36] F. Fuchs, J. Furthmüller, F. Bechstedt, M. Shishkin, and G. Kresse, Quasiparticle band structure based on a generalized Kohn-Sham scheme, Phys. Rev. B **76**, 115109 (2007).

[37] M. Gajdoš, K. Hummer, G. Kresse, J. Furthmüller, and F. Bechstedt, Linear optical properties in the projector-augmented wave methodology, Phys. Rev. B **73**, 045112 (2006).

[38] As temperature is not included in our simulations, energy is here to be interpreted as enthalpy at 0 K.

[39] M. Zinkevich, Thermodynamics of rare earth sesquioxides, Prog. Mater. Sci. **52**, 597 (2007).

[40] H. Yamashita, T. Broux, Y. Kobayashi, F. Takeiri, H. Ubukata, T. Zhu, M. A. Hayward, K. Fujii, M. Yashima, K. Shitara, A. Kuwabara, T. Murakami, and H. Kageyama, Chemical pressure-induced anion-order-disorder transition in LnHO enabled by hydride size flexibility, J. Am. Chem. Soc. **140**, 11170 (2018).

[41] Here we use the term metastability because this approach verifies the presence/absence of a local energy minimum associated with the anion-disordered phase. The most stable, or thermodynamically stable phase for a given composition is to be inferred by different energy consideration, such as in Figs. 3 and 4(a).

[42] N. Zapp, D. Sheptyakov, and H. Kohlmann, Computational chemistry-guided syntheses and crystal structures of the heavier lanthanide hydride oxides DyHO, ErHO, and LuHO, Crystals **11**, 750 (2021).

[43] P. v. Gelderen, P. A. Bobbert, P. J. Kelly, G. Brocks, and R. Tolboom, Parameter-free calculation of single-particle electronic excitations in YH_3, Phys. Rev. B **66**, 075104 (2002).

[44] A. T. M. van Gogh, D. G. Nagengast, E. S. Kooij, N. J. Koeman, J. H. Rector, R. Griessen, C. F. J. Flipse, and R. J. J. G. A. M. Smeets, Structural, electrical, and optical properties of $La_{1-z}Y_zH_x$ switchable mirrors, Phys. Rev. B **63**, 195105 (2001).

[45] V. Mudavakkat, V. Atuchin, V. Kruchinin, A. Kayani, and C. Ramana, Structure, morphology and optical properties of nanocrystalline yttrium oxide (Y_2O_3) thin films, Opt. Mater. (Amsterdam) **34**, 893 (2012).

[46] A. Prokofiev, A. Shelykh, and B. Melekh, Periodicity in the band gap variation of Ln_2X_3 (X = O, S, Se) in the lanthanide series, J. Alloys Compd. **242**, 41 (1996).

[47] F. Nafezarefi, H. Schreuders, B. Dam, and S. Cornelius, Photochromism of rare-earth metal-oxy-hydrides, Appl. Phys. Lett. **111**, 103903 (2017).

[48] S. Adalsteinsson, M. Moro, D. Moldarev, S. Droulias, M. Wolff, and D. Primetzhofer, Correlating chemical composition and optical properties of photochromic rare-earth oxyhydrides using ion beam analysis, Nucl. Instrum. Methods Phys. Res., Sect. B **485**, 36 (2020).

[49] D. Chaykina, F. Nafezarefi, G. Colombi, S. Cornelius, L. J. Bannenberg, H. Schreuders, and B. Dam, Influence of crystal structure, encapsulation, and annealing on photochromism in Nd oxyhydride thin Films, J. Phys. Chem. C **126**, 2276 (2022).

[50] J. P. Maehlen, T. T. Mongstad, C. C. You, and S. Karazhanov, Lattice contraction in photochromic yttrium hydride, J. Alloys Compd. **580**, S119 (2013).

[51] C. V. Chandran, H. Schreuders, B. Dam, J. W. G. Janssen, J. Bart, A. P. M. Kentgens, and P. J. M. van Bentum, Solid state NMR studies of the photochromic effects of thin films of oxygen containing yttrium hydride, J. Phys. Chem. C **118**, 22935 (2014).

[52] D. Chaykina, T. de Krom, G. Colombi, H. Schreuders, A. Suter, T. Prokscha, B. Dam, and S. Eijt, Structural properties and anion dynamics of yttrium dihydride and photochromic oxyhydride thin films examined by in situ μ^+SR, Phys. Rev. B **103**, 224106 (2021).

[53] E. M. Baba, P. M. Weiser, E. z. Zayim, and S. Karazhanov, Temperature-dependent photochromic performance of yttrium oxyhydride thin films, Phys. Status Solidi RRL **15**, 2000459 (2021).